



Divergent forest sensitivity to repeated extreme droughts

William R. L. Anderegg^{ID 1}✉, Anna T. Trugman^{ID 1,2}, Grayson Badgley^{ID 1}, Alexandra G. Konings^{ID 3} and John Shaw^{ID 4}

Climate change-driven increases in drought frequency and severity could compromise forest ecosystems and the terrestrial carbon sink^{1–3}. While the impacts of single droughts on forests have been widely studied^{4–6}, understanding whether forests acclimate to or become more vulnerable to sequential droughts remains largely unknown and is crucial for predicting future forest health. We combine cross-biome datasets of tree growth, tree mortality and ecosystem water content to quantify the effects of multiple droughts at a range of scales from individual trees to the globe from 1900 to 2018. We find that subsequent droughts generally have a more deleterious impact than initial droughts, but this effect differs enormously by clade and ecosystem, with gymnosperms and conifer-dominated ecosystems more often exhibiting increased vulnerability to multiple droughts. The differential impacts of multiple droughts across clades and biomes indicate that drought frequency changes may have fundamentally different ecological and carbon-cycle consequences across ecosystems.

Climate extremes have major impacts on the terrestrial carbon cycle^{1–3}. Climate models project increases in the frequency and severity of prominent climate extremes such as drought^{3,7,8}. Thus, the response of ecosystems to climate extremes represents an important uncertainty in carbon-cycle feedbacks and may have the potential to alter terrestrial ecosystems from a net sink to a carbon source over the twenty-first century^{2,3,9,10}. Severe droughts are one of the most consequential types of climate extremes when considering carbon-cycle impacts¹¹ and can have reverberating societal impacts. The effects of single extreme droughts have been widely studied, such as for severe droughts in Europe¹, North America⁴ and the Amazon⁵. By contrast, the ecosystem impacts of repeated extremes remain poorly understood. We remain unable to predict whether, after a severe drought, an ecosystem emerges more or less vulnerable to the next drought^{12–14}. Thus, understanding ecosystem response to multiple, repeated droughts is crucial for predicting long-term climate change impacts on ecosystems and the subsequent carbon-cycle feedbacks.

Ecosystem resilience to extreme droughts is an integrated combination of (1) the capacity of the ecosystem to persist and maintain its state and function during the disturbance, often called ‘sensitivity’ or ‘resistance’, and (2) the recovery trajectory following the disturbance^{15–17}. Multiple resilience-increasing and resilience-decreasing mechanisms exist at both organism (for example, tree) and ecosystem scales. The net impact of repeated droughts on Earth’s forests will depend on their balance. At a tree scale, adjustments in functional traits such as wood density or leaf turgor-loss thresholds or

in allometric patterns such as increased root or sapwood areas and decreased leaf area can improve tree resilience to future stress^{18,19}. By contrast, lingering drought-driven physiological damage such as embolism of the xylem, decreased reserves or defences, or pest/pathogen attacks and infections, among other mechanisms, may decrease tree resilience to subsequent droughts^{20,21}. At an ecosystem scale, forest density changes that lead to lower community-level water loss or changes in species composition that result in a more-drought-tolerant community may increase resilience^{6,22–24}. By contrast, microclimate feedbacks that drive hotter and drier canopy microenvironments, or landscape-scale pest or pathogen population dynamics triggered by an initial drought that lead to higher pest pressures on communities, could decrease resilience^{25–27}. Determining which of these mechanisms dominate under which circumstances and in which forest systems will be fundamental to predicting the future of Earth’s forests and their carbon-cycle feedbacks.

Here, we examine the drought sensitivity (that is, inverse of resistance) of forests to repeated droughts on the basis of growth increment at the tree level, mortality at the forest level and water content at the ecosystem level. When multiple droughts strike a forest, we predict that a system that exhibited increased sensitivity would experience larger growth declines, higher mortality rates and larger declines in canopy water content during a subsequent drought due to accumulated physiological damage from the initial drought. We leverage a cross-biome tree-ring dataset, long-term forest monitoring plots, satellite measurements of canopy water content and global drought datasets to quantify the effects of repeated droughts across scales. We quantify drought severity here from a climate perspective of the statistical distribution of drought metrics. We ask: (1) Are tree growth and mortality more, less or similarly sensitive to a subsequent drought compared with an initial drought? (2) Do changes in tree-level drought sensitivity differ by clade, biome or region? (3) Does drought sensitivity scale from the tree to ecosystem level, and how does this vary by biome and region? We analyse all ecological datasets at multiple levels of drought severity and use a number of approaches to control for potential confounding factors such as differences in drought severity (Methods).

We first examined tree growth patterns using a dataset of 1,208 stand growth chronologies spanning 1900–2015 from the International Tree-Ring Data Bank (ITRDB). On the basis of the Standardized Precipitation Evapotranspiration Index (SPEI), tree growth decline was larger in a subsequent drought at severe drought values ($P_{\text{SPEI} < -2} < 0.001$) and then converged to initial drought levels at more moderate drought values ($P_{\text{SPEI}(-1.5, -1.2]} = 0.33$) (Fig. 1a and Extended Data Fig. 1). This suggests a critical role of drought severity

¹School of Biological Sciences, University of Utah, Salt Lake City, UT, USA. ²Department of Geography, University of California Santa Barbara, Santa Barbara, CA, USA. ³Department of Earth System Science, Stanford University, Stanford, CA, USA. ⁴Rocky Mountain Research Station, United States Forest Service, Ogden, UT, USA. ✉e-mail: anderegg@utah.edu

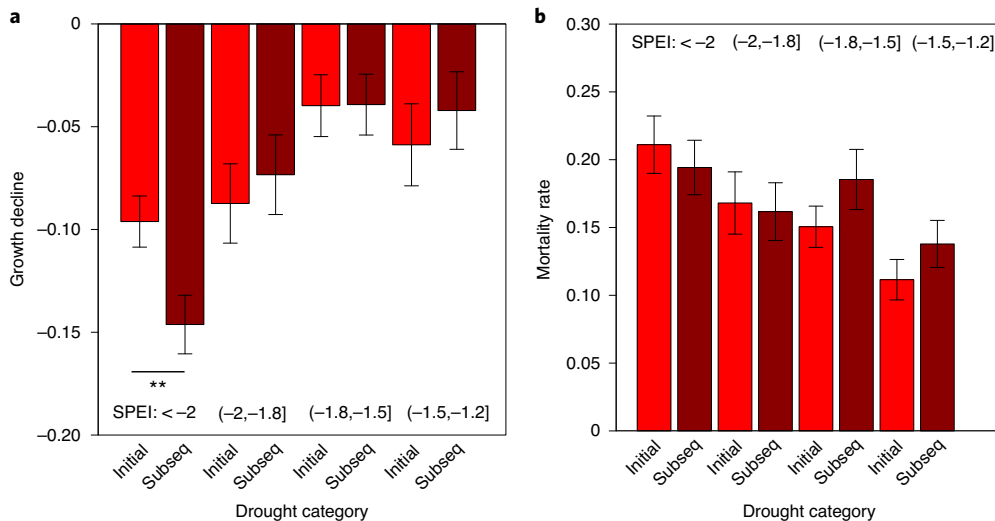


Fig. 1 | Impacts of a subsequent drought are more deleterious than an initial drought for trees. **a**, Growth declines (Δ ring-width index from 1,208 sites in the ITRDB) due to an initial drought (Initial, light red) and subsequent drought (Subseq, dark red), categorized by drought severity of both droughts via the SPEI (left to right, $N_{\text{chronologies}} = 516, 214, 347, 291$). **b**, Tree mortality rates ($\text{m}^2 \text{ha}^{-1} \text{yr}^{-1}$) across the US FIA plots due to initial and subsequent droughts (left to right, $N_{\text{plots}} = 6,414, 1,638, 2,781, 958; N_{\text{grid-cells}} = 140, 62, 112, 59$). Error bars indicate ± 1 standard error. Asterisks indicate statistically significant differences (** $P < 0.01$).

whereby an initial severe drought was associated with higher vulnerability to a subsequent severe drought, perhaps due to residual physiological damage. We next examined tree mortality patterns using the extensive US Forest Inventory and Analysis (FIA) dataset spanning $>100,000$ forested plots from 2000 to 2018. In contrast to the growth findings, we found that mortality was relatively similar between initial and subsequent droughts with no significant differences (for example, $P_{\text{SPEI} < -2} = 0.13$) (Fig. 1b). Drought severity between the initial and subsequent droughts was not significantly different and thus did not drive these patterns (Extended Data Fig. 2A,B). Tree-level drought sensitivity patterns held when accounting for differences in tree-ring analysis methods (Extended Data Fig. 3), multiple drought metrics (Extended Data Fig. 4) and spatial autocorrelation (Extended Data Fig. 5).

We then examined what factors mediated growth and mortality responses to multiple droughts. Clade (angiosperm–gymnosperm) and family were important predictors of tree-ring-based growth sensitivity differences to severe droughts ($P_{\text{clade}} = 0.0009$, ANOVA: $P_{\text{family}} = 0.01$) with gymnosperms and pine species (Pinaceae) exhibiting the highest sensitivity to subsequent droughts (Fig. 2a,b and Extended Data Fig. 1B). By contrast, angiosperms and oak species (Fagaceae) showed an ‘acclimation-type’ response where growth was less sensitive to subsequent drought than to the initial drought ($P = 0.03$) (Fig. 2a,b). Increased time between the initial and subsequent droughts was associated with smaller growth decline differences, although this effect was modest ($R^2 = 0.01$, $P = 0.02$). When examining mortality from forest inventory data in response to repeated droughts, angiosperm and gymnosperm sensitivities diverged at moderate drought severities ($P_{(-2, -1.8]} = 0.03$, $P_{(-1.8, -1.5]} = 0.01$). Gymnosperms appeared to show slightly elevated mortality in the initial drought at severe drought levels (for example, $P_{<-2} = 0.02$), whereas angiosperms exhibited higher mortality rates to subsequent droughts at more moderate drought levels ($P_{(-1.8, -1.5]} = 0.004$) (Fig. 2c). These contrasting clade patterns may explain the relatively muted mortality signal on the full dataset (Fig. 1b). We hypothesize that higher gymnosperm mortality during initial droughts may be due a ‘culling of the weak’ effect where death of the most vulnerable trees in a population results in less-vulnerable trees on average during subsequent droughts, potentially associated

with differences in biotic-agent attack differences between droughts (for example, higher beetle attack prevalence in initial droughts).

Both decreases in growth and increases in mortality are likely to negatively impact ecosystem resilience and carbon sequestration over the long term. Tree-bole growth provides a key ecosystem function of carbon storage in a pool with a long residence time (decades to centuries), although extrapolation of tree rings to whole-forest carbon is often challenging, and low growth can be a warning signal preceding large-scale mortality^{28,29}. Elevated mortality due to drought will have manifold ecological and carbon-cycle consequences, including changes in community composition and carbon sequestration²³. The higher mortality rate in subsequent droughts for angiosperms during moderate droughts (Fig. 2c) could be due to accumulated physiological damage²⁰ or because of ‘structural overshoot’ whereby these species might allocate too much carbon to leaf area during non-drought conditions, leading them to experience elevated mortality when drought strikes³⁰. We note, however, that the coarse temporal nature of inventory data adds uncertainty and is a caveat in our mortality rate analyses (Methods).

We further examined ecosystem-scale responses to multiple droughts via remotely sensed vegetation optical depth (VOD), which captures dynamics of canopy water content and ecosystem drought stress^{31,32}. Ecosystem-scale responses showed generally greater magnitudes and similar patterns to tree-level responses, with larger VOD declines in the subsequent drought that were most prominent at severe drought levels ($P_{\text{SPEI} < -2} < 0.0001$; $P_{\text{SPEI} (-1.5, -1.2]} < 0.001$) (Fig. 3a). In this dataset alone, we detected slight differences in drought severity between initial and subsequent droughts at severe drought levels (SPEI < -2 ; Extended Data Fig. 2C) and thus implemented multiple models to account for these differences (Methods). All of our patterns were robust when accounting for drought severity differences and drought legacy effects (Extended Data Figs. 6 and 7). At biome scales, temperate conifer forests and wet tropical forests showed the largest drought-severity-normalized increase in sensitivity in the second drought ($P < 0.001$ for both) (Figs. 3b and 4). The decrease in drought sensitivity in boreal forests and Mediterranean-type woodlands is intriguing and may be due to community turnover favouring more-drought-tolerant species³³. The Amazonian rainforest stands out as a region of increased

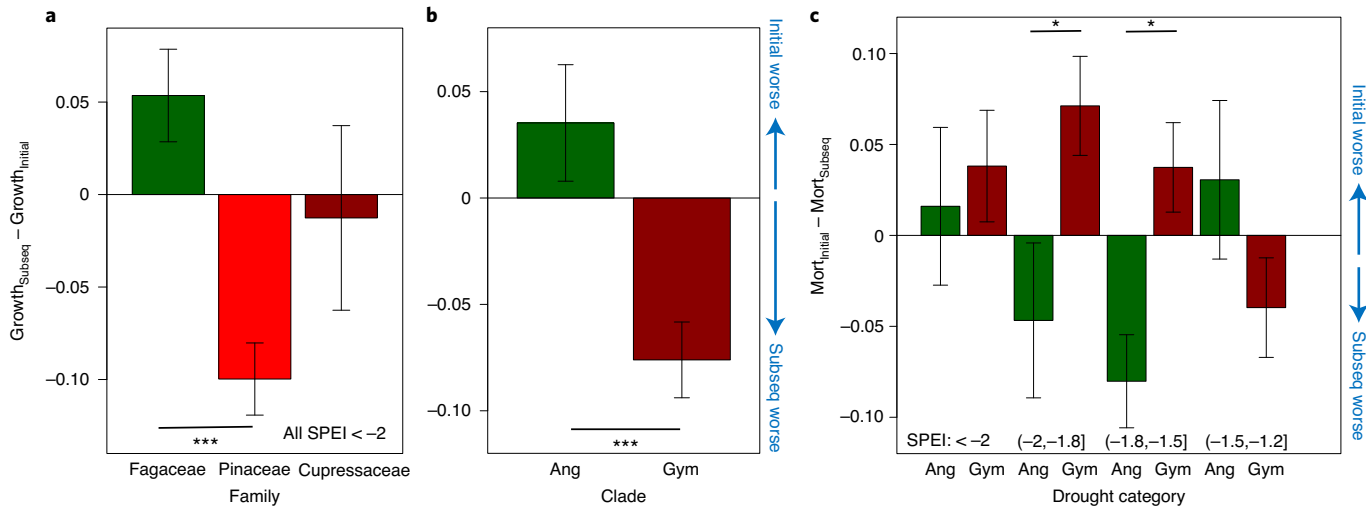


Fig. 2 | Impacts of multiple droughts on tree growth and mortality are mediated by clade. **a,b,** Growth decline differences from the ITRDB by family (**a**) and clade (**b**), where negative numbers indicate a more deleterious effect of the subsequent drought (left to right, $N_{\text{chronologies}} = 100, 332, 36, 106, 410$). **c,** Tree mortality differences across the US FIA plots between angiosperm-dominated (Ang, green) and gymnosperm-dominated (Gym, red) forests, with negative numbers indicating a more deleterious effect of the subsequent drought, categorized by drought severity of both droughts via the SPEI (left to right, $N_{\text{plots}} = 2,740, 3,674, 1,011, 627, 1,980, 801, 868, 90$). Error bars indicate ± 1 standard error. Asterisks indicate statistically significant differences (* $P < 0.05$; ** $P < 0.01$; *** $P < 0.001$). Note that the order of subtraction is different among **a**, **b** and **c** to maintain the convention that negative values indicate a more deleterious impact of the subsequent drought across all panels.

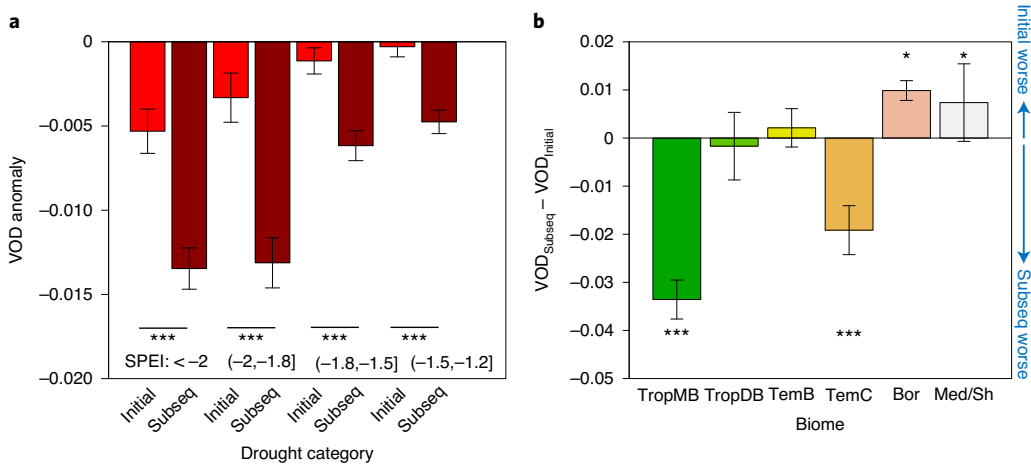


Fig. 3 | Ecosystem impacts of a subsequent drought are more deleterious than an initial drought. **a,** VOD anomaly in response to an initial drought (Initial, light red) and subsequent drought (Subseq, dark red), categorized by drought severity of both droughts via the SPEI thresholds (left to right, $N_{\text{grid-cells}} = 745, 425, 1,491, 2,398$). **b,** Differences in VOD anomalies during a drought of SPEI < -2 across different forest biomes between initial and subsequent droughts, with negative numbers indicating a more deleterious effect of the subsequent drought. TropMB, tropical moist broadleaf; TropDB, tropical dry broadleaf; TemB, temperate broadleaf; TemC, temperate conifer; Bor, boreal; Med/Sh, Mediterranean-type shrubland (left to right, $N_{\text{grid-cells}} = 248, 50, 89, 46, 291, 21$). Error bars indicate ± 1 standard error. Asterisks indicate statistically significant differences (* $P < 0.05$; ** $P < 0.01$; *** $P < 0.001$).

sensitivity, which is highly relevant because the Amazon experienced two very severe droughts in 2005 and 2010, which had widely documented effects on growth, mortality and carbon cycling in the region^{5,34}. Given the importance of the Amazon in the global carbon cycle³⁵, and that climate projections indicate increased vapour pressure deficit (atmospheric dryness) and in some cases rainfall reductions in this region³⁶, increased sensitivity to repeated droughts is of critical concern (Fig. 4).

While forests on average showed increasing sensitivity to a subsequent drought, forests diverged enormously and with several broad patterns that were revealed across diverse datasets spanning

a wide range of spatial and temporal scales. Angiosperm trees and angiosperm-dominated forests tended to show more acclimation (decreased sensitivity) responses. By contrast, gymnosperms tended to exhibit more stress accumulation (increased sensitivity) responses, except for mortality. These patterns are consistent with anatomical and physiological differences between these two clades. Angiosperms have much higher anatomical flexibility than gymnosperms, for example, in terms of xylem anatomy, parenchyma fractions and whole-plant allocation patterns, that allows angiosperms far more plastic responses when faced with drought^{37,38}. Our results are broadly consistent with a recent study³⁹ that found differences in

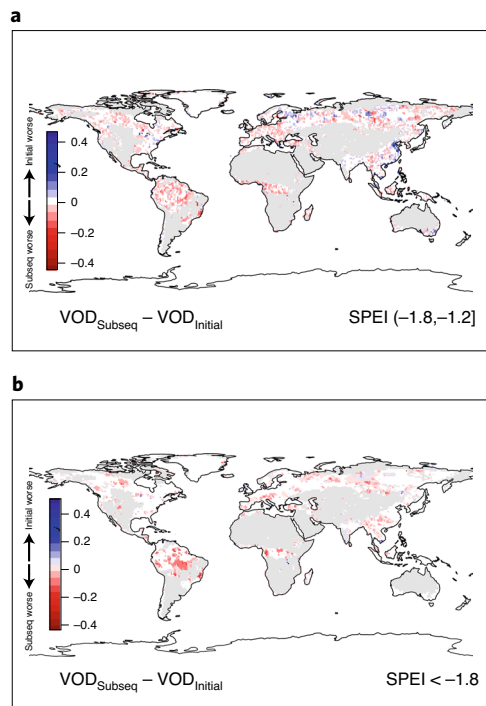


Fig. 4 | Ecosystem impacts of a subsequent drought compared with an initial drought diverge across global forests. **a,b,** VOD anomalies in response to a subsequent drought (Subseq) minus an initial drought (Initial), with red colours indicating a more deleterious effect of the second drought, categorized by drought severity of both droughts via the SPEI thresholds of a moderate drought (SPEI $(-1.8, -1.2]$) (**a**) or severe drought (SPEI < -1.8) (**b**). Grey areas indicate regions not dominated by forests; white areas in **b** indicate that two droughts exceeding that SPEI severity did not occur in the record.

gymnosperms' and angiosperms' growth responses to drought were linked to subsequent mortality risk, although our analyses examine a greater number of sites and diversity of biomes and include ecosystem-level assessments of multiple drought impacts as well. Changes in competition, light environment and pest/pathogen dynamics—for example, co-occurring drought and beetle outbreaks have been widely observed in western US gymnosperm species and could drive high mortality levels in initial droughts when stand densities are higher—are other potential mechanisms that might give rise to these responses. One notable exception to the broad clade patterns, however, was the strong increases in sensitivity observed in canopy water content in the Amazon between two severe and closely timed droughts, which might indicate that drought severity and timing overwhelmed the acclimation responses. Further detailed and long-term studies on tree physiology and forest demography are greatly needed to elucidate and test the various mechanisms that might underlie these patterns.

Current vegetation and Earth system models largely do not contain the major potential mechanisms, such as accumulated physiological damage or pest/pathogen infections, that might generate the patterns observed here. However, representations of physiological processes of drought stress, such as plant hydraulics and forest demography, are major priorities in Earth system model development^{24,40,41}. These advances hold substantial promise for improving Earth system model simulation of the response of forests to single severe droughts^{24,42}. Our results highlight that we must also consider including mechanisms that might mediate changes in forest responses to repeated droughts. For example, trait plasticity and allocation changes based on mechanistic understanding

are currently possible to include in large-scale models^{43,44} and may enable capturing the responses documented here. We hypothesize that both trait plasticity and clade-specific limits to plasticity have potential to capture the differential responses documented here. Our results further indicate that broad functional-type categories may be useful in setting the limits and directions of changes in acclimation and plasticity.

We have shown both at an individual tree scale and at an ecosystem scale that the response to repeated droughts can diverge from that of a single drought. While there are a few cases of similar or decreasing sensitivity to a subsequent drought, we generally see increased vulnerability to a subsequent drought. These responses were strongly mediated by the clade and family, with gymnosperms broadly showing much higher vulnerability to subsequent droughts. Given projected increases in drought frequency in the twenty-first century in many regions, our findings point towards decreasing ecosystem resilience, in the near term at least, that may portend ill news for the land carbon sink and Earth's forests in future climates.

Online content

Any methods, additional references, Nature Research reporting summaries, source data, extended data, supplementary information, acknowledgements, peer review information; details of author contributions and competing interests; and statements of data and code availability are available at <https://doi.org/10.1038/s41558-020-00919-1>.

Received: 16 January 2020; Accepted: 2 September 2020;

Published online: 28 September 2020

References

- Ciais, P. et al. Europe-wide reduction in primary productivity caused by the heat and drought in 2003. *Nature* **437**, 529–533 (2005).
- Reichstein, M. et al. Climate extremes and the carbon cycle. *Nature* **500**, 287–295 (2013).
- IPCC Special Report on Managing the Risks of Extreme Events and Disasters to Advance Climate Change Adaptation (eds Field, C. B. et al.) (Cambridge Univ. Press, 2012).
- Schalm, C. R. et al. Reduction in carbon uptake during turn of the century drought in western North America. *Nat. Geosci.* **5**, 551–556 (2012).
- Phillips, O. L. et al. Drought sensitivity of the Amazon rainforest. *Science* **323**, 1344–1347 (2009).
- Allen, C. D., Breshears, D. D. & McDowell, N. G. On underestimation of global vulnerability to tree mortality and forest die-off from hotter drought in the Anthropocene. *Ecosphere* **6**, 129 (2015).
- Dai, A. Drought under global warming: a review. *Wiley Interdiscip. Rev. Clim. Change* **2**, 45–65 (2011).
- Cook, B. I., Smerdon, J. E., Seager, R. & Coats, S. Global warming and 21st century drying. *Clim. Dyn.* **43**, 2607–2627 (2014).
- Cox, P. M., Betts, R. A., Jones, C. D., Spall, S. A. & Totterdell, I. J. Acceleration of global warming due to carbon-cycle feedbacks in a coupled climate model. *Nature* **408**, 184–187 (2000).
- Friedlingstein, P. et al. Uncertainties in CMIP5 climate projections due to carbon cycle feedbacks. *J. Clim.* **27**, 511–526 (2014).
- Zscheischler, J. et al. A few extreme events dominate global interannual variability in gross primary production. *Environ. Res. Lett.* **9**, 035001 (2014).
- Miao, S., Zou, C. B. & Breshears, D. D. Vegetation responses to extreme hydrological events: sequence matters. *Am. Nat.* **173**, 113–118 (2008).
- Anderegg, W. R. L. et al. Pervasive drought legacies in forest ecosystems and their implications for carbon cycle models. *Science* **349**, 528–532 (2015).
- Schalm, C. R. et al. Global patterns of drought recovery. *Nature* **548**, 202–205 (2017).
- Holling, C. S. Resilience and stability of ecological systems. *Annu. Rev. Ecol. Syst.* **4**, 1–23 (1973).
- Gunderson, L. H. et al. Ecological resilience—in theory and application. *Annu. Rev. Ecol. Syst.* **31**, 425–439 (2000).
- Ingrisch, J. & Bahn, M. Towards a comparable quantification of resilience. *Trends Ecol. Evol.* **33**, 251–259 (2018).
- Bartlett, M. K. et al. Global analysis of plasticity in turgor loss point, a key drought tolerance trait. *Ecol. Lett.* **17**, 1580–1590 (2014).
- Martínez-Vilalta, J. et al. Hydraulic adjustment of Scots pine across Europe. *New Phytol.* **184**, 353–364 (2009).

20. Hacke, U. G., Stiller, V., Sperry, J. S., Pittermann, J. & McCulloh, K. A. Cavitation fatigue. Embolism and refilling cycles can weaken the cavitation resistance of xylem. *Plant Physiol.* **125**, 779–786 (2001).
21. Sala, A., Woodruff, D. R. & Meinzer, F. C. Carbon dynamics in trees: feast or famine? *Tree Physiol.* **32**, 764–775 (2012).
22. Schymanski, S. J., Roderick, M. L., Sivapalan, M., Hutley, L. B. & Beringer, J. A canopy-scale test of the optimal water-use hypothesis. *Plant Cell Environ.* **31**, 97–111 (2008).
23. Zhang, T., Niinemets, Ü., Sheffield, J. & Lichstein, J. W. Shifts in tree functional composition amplify the response of forest biomass to climate. *Nature* **556**, 99–102 (2018).
24. Anderegg, W. R. et al. Hydraulic diversity of forests regulates ecosystem resilience during drought. *Nature* **561**, 538–541 (2018).
25. Royer, P. D. et al. Extreme climatic event-triggered overstorey vegetation loss increases understorey solar input regionally: primary and secondary ecological implications. *J. Ecol.* **99**, 714–723 (2011).
26. Raffa, K. F. et al. Cross-scale drivers of natural disturbances prone to anthropogenic amplification: the dynamics of bark beetle eruptions. *BioScience* **58**, 501–517 (2008).
27. Anderegg, W. R., Trugman, A. T., Bowling, D. R., Salvucci, G. & Tuttle, S. E. Plant functional traits and climate influence drought intensification and land-atmosphere feedbacks. *Proc. Natl Acad. Sci. USA* **116**, 14071–14076 (2019).
28. Cailleret, M. et al. A synthesis of radial growth patterns preceding tree mortality. *Glob. Change Biol.* **23**, 1675–1690 (2017).
29. Camarero, J. J., Gazol, A., Sangüesa-Barreda, G., Oliva, J. & Vicente-Serrano, S. M. To die or not to die: early warnings of tree dieback in response to a severe drought. *J. Ecol.* **103**, 44–57 (2015).
30. Jump, A. S. et al. Structural overshoot of tree growth with climate variability and the global spectrum of drought-induced forest dieback. *Glob. Change Biol.* **23**, 3742–3757 (2017).
31. Saatchi, S. et al. Persistent effects of a severe drought on Amazonian forest canopy. *Proc. Natl Acad. Sci. USA* **110**, 565–570 (2013).
32. Konings, A. G., Williams, A. P. & Gentine, P. Sensitivity of grassland productivity to aridity controlled by stomatal and xylem regulation. *Nat. Geosci.* **10**, 284–288 (2017).
33. Carnicer, J. et al. Widespread crown condition decline, food web disruption, and amplified tree mortality with increased climate change-type drought. *Proc. Natl Acad. Sci. USA* **108**, 1474–1478 (2011).
34. Brienen, R. J. W. et al. Long-term decline of the Amazon carbon sink. *Nature* **519**, 344–348 (2015).
35. Lenton, T. M. et al. Tipping elements in the Earth's climate system. *Proc. Natl Acad. Sci. USA* **105**, 1786–1793 (2008).
36. Duffy, P. B., Brando, P., Asner, G. P. & Field, C. B. Projections of future meteorological drought and wet periods in the Amazon. *Proc. Natl Acad. Sci. USA* **112**, 13172–13177 (2015).
37. Johnson, D. M., McCulloh, K. A., Woodruff, D. R. & Meinzer, F. C. Hydraulic safety margins and embolism reversal in stems and leaves: why are conifers and angiosperms so different? *Plant Sci.* **196**, 48–53 (2012).
38. Morris, H. et al. A global analysis of parenchyma tissue fractions in secondary xylem of seed plants. *New Phytol.* **209**, 1553–1565 (2016).
39. DeSoto, L. et al. Low growth resilience to drought is related to future mortality risk in trees. *Nat. Commun.* **11**, 1–9 (2020).
40. Fisher, R. A. et al. Vegetation demographics in Earth system models: a review of progress and priorities. *Glob. Change Biol.* **24**, 35–54 (2018).
41. Kennedy, D. et al. Implementing plant hydraulics in the Community Land Model, version 5. *J. Adv. Model. Earth Syst.* **11**, 485–513 (2019).
42. Trugman, A. T. et al. Tree carbon allocation explains forest drought-kill and recovery patterns. *Ecol. Lett.* **21**, 1552–1560 (2018).
43. Trugman, A. T. et al. Climate and plant trait strategies determine tree carbon allocation to leaves and mediate future forest productivity. *Glob. Change Biol.* **25**, 3395–3405 (2019).
44. Scheiter, S., Langan, L. & Higgins, S. I. Next-generation dynamic global vegetation models: learning from community ecology. *New Phytol.* **198**, 957–969 (2013).

Publisher's note Springer Nature remains neutral with regard to jurisdictional claims in published maps and institutional affiliations.

© The Author(s), under exclusive licence to Springer Nature Limited 2020

Methods

Drought datasets. We used the SPEI as our primary drought metric in this study for several reasons. First, as an agricultural drought index, SPEI integrates both water supply through precipitation and water demand through potential evapotranspiration (PET), which makes it a simple and physiologically relevant drought index based on a water budget that is more relevant to ecosystem water stress than are meteorological drought indices based only on precipitation and temperature^{45–47}. SPEI has been widely used to assess ecosystem response to drought at multiple spatial and temporal scales^{1,4,48}. Second, unlike other agricultural drought metrics such as the Palmer Drought Severity Index, SPEI is standardized within each grid cell to a mean of zero and standard deviation of one with a Gaussian distribution⁴⁶. Thus, drought severity can be quantitatively compared across regions and ecosystems, normalized by each grid cell's climatology. Finally, current publicly available datasets of SPEI contain global coverage of drought data over the full historical record (1900–2019)⁴⁵, enabling us to maximize the sample size of ecological data collected over 1900–2018.

We downloaded the full SPEI Global Drought Monitor dataset on 1 March 2019, which provides global SPEI data at 1° resolution from 1900 to 2019^{45,46}. This dataset uses the precipitation data from the Global Precipitation Climatology Centre and calculates PET using a Thornthwaite algorithm, with temperature based on the National Oceanic and Atmospheric Administration National Center for Environmental Prediction's Global Historical Climatology Network dataset⁴⁷. Because the Thornthwaite PET calculation is a simplification, we also performed analyses with SPEI calculated via the more robust Penman-Monteith PET algorithm in the Global SPEI Database⁴⁵. We observed very similar patterns, and because the SPEI Global Drought Monitor Database covers 1900–2019 (as opposed to 1900–2015 for the SPEI Global Database), we used it for our primary analysis. SPEI can be calculated with respect to different 'integration windows' over which drought severity is calculated and normalized to the climatological period⁴⁸. We chose a 12-month integration window because an annual time step is consistent with both the tree-ring and forest inventory plot datasets. We calculated 12-month SPEI values for both calendar year and water year (October–September) in the Northern Hemisphere and observed very similar results in the tree-ring analysis; we thus present calendar-year results in all figures.

For all analyses, we examined four levels of drought severity that span a range from moderate to severe drought. We chose SPEI drought-severity bins of $[-1.2, -1.5]$, $[-1.5, -1.8]$, $[-1.8, -2]$ and < -2.0 for these drought-severity levels. Because SPEI values are based on z scores, an SPEI value of -2.0 indicates a 2 s.d. drought. This range of values allowed us to assess whether ecosystem response to moderate drought differed from that of severe droughts.

Tree-ring analysis. To quantify tree growth responses to multiple droughts, we used tree-ring chronologies from the extensive ITRDB. The ITRDB is a publicly available dataset that contains tree-ring chronologies for >2,000 sites around the world. Following a recent global analysis that examined drought recovery periods in ITRDB tree-ring chronologies³, we analysed 1,208 chronologies that had standard formatting and included at least 25 years in the observational record (1900–2018) (Extended Data Fig. 8). These chronologies span >40 species and a wide array of temperate and boreal forest types, although they are concentrated in the Northern Hemisphere, primarily in North America and Europe. For each chronology, we analysed the detrended ring-width index where detrending had been performed by the individual data contributor of that chronology, following previous studies^{13,49}.

On the basis of the latitude and longitude coordinates of each chronology, we calculated the ring-width reduction during the first two droughts that exceeded the given drought threshold in each chronology. We imposed a criterion that the two droughts had to be temporally separated by more than 2 years with SPEI values above the drought threshold to avoid counting multi-year single droughts as two different droughts. This minimum gap between droughts is based on previous research on these tree-ring chronologies that indicated that drought legacy effects typically lasted 1–2 years (ref. ¹³), and thus our analysis avoids these effects. For a given drought event, if multiple years in a row exceeded the drought threshold, we used the ring width of the final year of the drought. For example, for a drought threshold of SPEI < -2 , if a given chronology experienced an SPEI time series of 0, -2.2 , -2.1 , 0, -2.1 and no other droughts, it would not be used due to insufficient time between two droughts. If the SPEI time series were 0, -2.2 , -2.1 , 0, 0, -2.1 , then year 3 would be calculated as 'drought 1' and year 6 as 'drought 2'. These criteria allowed us to assess the impact of multiple droughts while avoiding a potential confounding effect of analysing 2 years in essentially the same individual drought. We did a sensitivity analysis on both the drought-severity recovery threshold (for example, recovery threshold of SPEI > -1.2 , SPEI > 0 and so on) and 1–4 years of recovery period, and neither had a major effect on our results. We did not include an upper limit to the time between two droughts because several of the hypothesized ecological and physiological mechanisms that might mediate changes in tree sensitivity to drought, such as changes in canopy architecture, allocation or species composition, certainly operate on multi-decadal timescales²³. Individual chronologies could occur in multiple drought-severity bins if they experienced four droughts or more. We note that we did not explicitly include drought duration in these analyses, but we do not think it would likely

influence our results given that we observed similar patterns across a wide suite of sensitivity analyses.

We detected no systematic differences in drought severity between initial and subsequent droughts in the ITRDB dataset (Extended Data Fig. 2). It is also highly unlikely that trends in ring width due to ontogeny/stand development, given that tree-ring chronologies are detrended to explicitly remove such patterns, or trends in drought metrics might confound our results. Nevertheless, we conducted a sensitivity analysis to ensure that detrending and/or removal of an autoregressive model ('prewhitening') did not influence our results. In this analysis, we compared the 'standardized' chronology (.crn file) in ITRDB used in Fig. 1 with application of a single, consistent detrending spline method or a single, consistent detrending and prewhitening method (methods 'spline' and 'ar', respectively, in the detrend. series function standard settings in dplR), and our results were robust (Extended Data Fig. 3). In addition, because only a subset of species in a given region or community yield easily readable tree-ring series, this may amplify the phylogenetic drought response observed here. Finally, we note that the chronologies in the ITRDB dataset are not randomly distributed and tend to overestimate climate sensitivity due to site selection compared with randomly distributed inventory plots⁵⁰, but this should not greatly influence our results. This is because spatial or population biases in ITRDB (higher climate sensitivities) would give, on average, a greater decline in growth during any given drought but should not, *a priori*, affect the temporal changes in growth responses between multiple droughts within the same chronology. This site selection bias would make scaling ITRDB tree-ring chronologies to whole-forest carbon pools challenging, however, and thus we use only VOD for whole-ecosystem assessments here.

Forest inventory analysis. To quantify tree mortality responses to multiple droughts, we used the US Forest Service FIA long-term permanent plot network. The FIA network contains >250,000 permanent plots on all lands with at least 10% tree cover in the contiguous United States^{51–53}. Since the plot protocols were standardized nationwide in 2000, FIA plots are set up on a stratified random sampling design, and tree status (living/dead) is measured on a plot return interval that varies by state, typically every 5 years (that is, 20% of plots censused each year) in the eastern United States and every 10 years (that is, 10% of plots censused each year) in the western United States^{51–53}. This means that as of 2018, many eastern states have three to four censuses and many western states have one to two censuses. States in the Intermountain West FIA region (Colorado, Arizona, New Mexico, Utah, Idaho, Montana) also estimated a mortality in the past 5 years during the initial census of plots, which allows these states' inventory plots with two censuses to be used in this study because the plots contain two mortality rates (that is, mortality rate 0–5 years before census 1 and a mortality rate between census 1 and census 2). Thus, while FIA data in both the western United States and eastern United States can be used for this analysis, we note that limitations associated with relatively sparse temporal sampling of FIA remains an uncertainty and caveat.

We calculated total basal area mortality for forested plots with FIA plot condition classes that occupied >30% of a given plot area. Plots with fire damage, human damage, and treatments (for example, timber harvesting) were excluded. For all states with 3+ censuses, we calculated mortality rates using the basal area mortality documented in the return census and measured plot return interval. For Intermountain West states with only two censuses, we calculated the initial mortality rate using the 'estimated' 5-year mortality rate in the first census and then the documented mortality between the first and second censuses. This estimated mortality is determined by the FIA field crew during the first census as all trees that have died in the past 5 years on the basis of crown decay conditions and has been validated^{54,55}, but we note that our results were robust to excluding plots with estimated mortality (Extended Data Fig. 9). We then implemented a similar algorithm to detect plots where two droughts of a given severity level had occurred. Specifically, we analysed plots that had at least two mortality rate estimates and where each drought that exceeded the selected threshold had occurred in the 5 years before the census. When more than two droughts occurred at a plot, we analysed the first and second droughts similarly to the tree-ring analysis, provided the droughts were in different census intervals.

While there are many potential drivers of mortality rates in US forests, our analysis aimed to screen out major alternative confounding drivers, and drought has been identified in a wide body of literature of having a major impact on tree mortality in both eastern and western US forests since 2000^{23,56–58}, which can be widely observed in FIA plot mortality rates^{23,56,59}. We further analysed mortality responses to multiple droughts by forest type, using the FIA 'Field type code' variable, to categorize plots as angiosperm-dominated or gymnosperm-dominated forests. In addition, we detected no significant differences in drought severity between initial and subsequent at all drought-severity levels in FIA data (Extended Data Fig. 2B), indicating that differences in drought severity were unlikely to drive our results.

Satellite VOD analysis. VOD is a measure of the degree to which greybody emission from the surface of the Earth attenuates as it passes through both the woody and leafy components of the vegetation canopy. It is sensitive to canopy water content⁶⁰ and thus varies with both biomass^{61,62} and water stress^{63,64}. The constant of proportionality between VOD and canopy water content is

poorly understood. However, it appears to vary primarily with canopy type and electromagnetic frequency, suggesting it is relatively constant for a given land cover type⁶⁵. At the annual and longer timescales considered here, variations in VOD can be interpreted as due to variations in biomass growth and mortality⁶⁶. Here, we use VOD from the Land Parameter Data Record⁶⁷, which is retrieved from brightness temperatures measured by the Advanced Microwave Scanning Radiometer–Enhanced (AMSR-E) and Advanced Microwave Scanning Radiometer 2 (AMSR-2). For full details on the retrieval methods, see refs. ^{68–70}. We used data from January 2003 to December 2018.

We aggregated annual VOD values to the same resolution (1°) as the SPEI drought dataset and subtracted the grid-cell mean VOD to generate a time series of VOD anomalies in each grid cell. Similar to the tree-ring analysis, we searched the SPEI time series for each grid cell that contained two or more drought years that fell within the same SPEI drought-severity bins. We further constrained this such that the grid cell had to have at least one non-drought year between the two drought years to avoid counting the same multi-year drought as two individual drought events. We performed a sensitivity analysis of detrending individual VOD grid cells to ensure that directional trends, potentially due to other drivers such as land-use change, were not driving our results and our findings were robust (Extended Data Fig. 10). We used the biome map of Olson et al.⁷¹ to analyse VOD responses over forest and woodland biomes only (Fig. 3a) and to analyse impacts by individual biomes (Fig. 3b). While the VOD record is relatively short, it is similar in length to the FIA plot network, and there are multiple regions in the world where two moderate or severe droughts occurred (Fig. 4), including two 1-in-100-year droughts in the Amazon rainforest^{5,34}. Thus, it provides an integrated assessment of ecosystem-level drought impacts for many forest biomes across the globe^{24,31,32}.

We detected significant differences in drought severity between the initial and subsequent droughts in VOD grid cells that experienced two droughts for severe drought levels (see Analyses and statistics) (Extended Data Fig. 2), which must be accounted for to estimate ecosystem changes in sensitivity to drought between multiple droughts. We took two separate approaches to accounting for these drought-severity differences. First, we performed an analysis where we considered only VOD grid cells where the SPEI values were nearly identical (that is, within 0.1 of each other) for both droughts. Second, we built a model that accounted for drought severity in each grid cell. For each grid cell, we constructed an ordinary least squares regression between annual values of VOD anomaly and SPEI using a linear or quadratic relationship. We then calculated the relative drought impact of the first and second droughts in that grid cell as the residual of the drought years' VOD values from the regression, which subtracts out the effect of drought severity. Both approaches—and both functional forms in the second approach—revealed the similar findings that the impact of a second drought on ecosystem VOD was more severe than that of the first drought (Extended Data Fig. 6), indicating that the result is robust even when accounting for drought-severity differences.

To ensure that our results were not influenced by substantial drought legacy effects in VOD, we calculated the VOD anomaly for each grid cell in the 1–7 years following droughts of severity SPEI ($-2, -1.2$) or SPEI < -2 . We observed minor legacy effects lasting 1 year for SPEI ($-2, -1.2$) droughts and moderate legacy effects lasting 3 years for SPEI < -2 droughts. We conducted a sensitivity analysis where initial and subsequent droughts had to be separated by 3 years or more and observed that our findings were robust (Extended Data Fig. 7), indicating that our results are robust to drought legacy effects in VOD.

Analyses and statistics. For each of the three datasets (tree rings, forest inventory plots, VOD), we analysed the impacts of the initial drought versus the subsequent drought using either paired *t* tests (tree ring, VOD) or Wilcoxon signed rank tests (FIA) when data could not be transformed to meet assumptions of normality. Tree-ring and VOD data were often transformed using an arctangent transformation. We note that we do not test for differences in tree or ecosystem sensitivity across drought-severity categories (that is, we test only for sensitivity differences between an initial and subsequent drought at the same drought-severity level), and we used a Sidak correction for multiple hypothesis testing within each dataset's analyses where necessary⁷². We ensured that assumptions of normality and homogeneity of variances were met with Q–Q plots via the qqPlot diagnostic in the ‘car’ R package^{73,74}.

To ensure that tree or ecosystem sensitivity to multiple droughts was not driven by systematic drought-severity differences, we tested for differences in drought severity using Wilcoxon signed rank tests. Statistically significant differences were detected only in the VOD dataset at SPEI < -2 drought severities ($P = 0.005$) and were addressed as described in the preceding.

We tested for spatial autocorrelation in the differences between the initial and subsequent drought impacts using Moran's I^75 and found significant positive spatial autocorrelation in all three datasets ($P < 0.01$). In the tree-ring and VOD datasets, autocorrelation was addressed by using spatial autoregressive models that model the correlation structure of the data, using the gls function in the ‘nlme’ R package⁷⁶. Per standard practice⁷⁵, we included the latitude and longitude coordinates of each grid cell in the regression and tested the following spatial correlation structures—linear, quadratic ratio, exponential, spherical and Gaussian—selecting the most likely and parsimonious model using the difference in Akaike information criterion of < -2 or more. The quadratic or exponential

correlation structure was typically selected as most parsimonious. For FIA data, no transformations could achieve reasonable Q–Q plots for any family of generalized linear model, and thus we first averaged individual plot values at a 1° grid to account for spatial autocorrelation and then subsequently modelled the correlation structure. All results were robust to accounting for spatial autocorrelation (Extended Data Fig. 5). All analyses were conducted in the R statistical software⁷⁷.

Data availability

All datasets are publicly available. The International Tree-Ring Data Bank is available from the National Oceanic and Atmospheric Administration (<https://www.ncdc.noaa.gov/data-access/paleoclimatology-data/datasets/tree-ring>); the US Forest Inventory and Analysis plot data are available from the US Department of Agriculture (<https://www.fia.fs.fed.us/>); and the vegetation optical depth data are available from the University of Montana (<https://www.ntsg.umt.edu/project/default.php>).

Code availability

All analysis was done in the open-source software R with the packages that are documented and cited in the Methods section of the paper. Code will be made available on request.

References

45. Vicente-Serrano, S. M., Beguería, S., López-Moreno, J. I., Angulo, M. & El Kenawy, A. A new global 0.5 gridded dataset (1901–2006) of a multiscalar drought index: comparison with current drought index datasets based on the Palmer Drought Severity Index. *J. Hydrometeorol.* **11**, 1033–1043 (2010).
46. Beguería, S., Vicente-Serrano, S. M. & Angulo-Martínez, M. A multiscalar global drought dataset: the SPEIbase: a new gridded product for the analysis of drought variability and impacts. *Bull. Am. Meteorol. Soc.* **91**, 1351–1356 (2010).
47. Beguería, S., Vicente-Serrano, S. M., Reig, F. & Latorre, B. Standardized Precipitation Evapotranspiration Index (SPEI) revisited: parameter fitting, evapotranspiration models, tools, datasets and drought monitoring. *Int. J. Climatol.* **34**, 3001–3023 (2014).
48. Vicente-Serrano, S. M. et al. Response of vegetation to drought time-scales across global land biomes. *Proc. Natl Acad. Sci. USA* **110**, 52–57 (2013).
49. Gazol, A., Camarero, J. J., Anderegg, W. R. L. & Vicente-Serrano, S. M. Impacts of droughts on the growth resilience of Northern Hemisphere forests. *Glob. Ecol. Biogeogr.* **26**, 166–176 (2017).
50. Klesse, S. et al. Sampling bias overestimates climate change impacts on forest growth in the southwestern United States. *Nat. Commun.* **9**, 5336 (2018).
51. Bechtold, W. A. & Patterson, P. L. *The Enhanced Forest Inventory and Analysis Program—National Sampling Design and Estimation Procedures General Technical Report SRS-80* (USDA, 2005).
52. Bechtold, W. & Scott, C. T. in *The Enhanced Forest Inventory and Analysis Program—National Sampling Design and Estimation Procedures General Technical Report SRS-80* (eds Bechtold, W. A. & Patterson, P. L.) 37–52 (USDA, 2005).
53. Woudenberg, S. W. et al. *The Forest Inventory and Analysis Database: Database Description and Users Manual Version 4.0 for Phase 2* General Technical Report RMRS-GTR-245 (USDA, 2010).
54. Jacobi, W. R., Kearns, H. S. J. & Johnson, D. W. Persistence of pinyon pine snags and logs in southwestern Colorado. *West. J. Appl. For.* **20**, 247–252 (2005).
55. Shaw, J. D. et al. *Arizona's Forest Resources, 2001–2014 Resource Bulletin RMRS-RB-25* (USDA, 2018).
56. Shaw, J. D., Steed, B. E. & DeBlander, L. T. Forest inventory and analysis (FIA) annual inventory answers the question: what is happening to pinyon-juniper woodlands? *J. For.* **103**, 280–285 (2005).
57. Breshears, D. D. et al. Regional vegetation die-off in response to global-change-type drought. *Proc. Natl Acad. Sci. USA* **102**, 15144–15148 (2005).
58. Williams, A. P. et al. Forest responses to increasing aridity and warmth in the southwestern United States. *Proc. Natl Acad. Sci. USA* **107**, 21289–21294 (2010).
59. Anderegg, W. R. et al. Tree mortality from drought, insects, and their interactions in a changing climate. *New Phytol.* **208**, 674–683 (2015).
60. Jackson, T. J. & Schmugge, T. J. Vegetation effects on the microwave emission of soils. *Remote Sens. Environ.* **36**, 203–212 (1991).
61. Tian, F. et al. Remote sensing of vegetation dynamics in drylands: evaluating vegetation optical depth (VOD) using AVHRR NDVI and in situ green biomass data over West African Sahel. *Remote Sens. Environ.* **177**, 265–276 (2016).
62. Liu, Y. Y. et al. Recent reversal in loss of global terrestrial biomass. *Nat. Clim. Change* **5**, 470–474 (2015).
63. Momen, M. et al. Interacting effects of leaf water potential and biomass on vegetation optical depth. *J. Geophys. Res. Biogeosci.* **122**, 3031–3046 (2017).

64. Konings, A. G. & Gentine, P. Global variations in ecosystem-scale isohydricity. *Glob. Change Biol.* **23**, 891–905 (2017).
65. Van de Griend, A. A. & Wigneron, J.-P. The b-factor as a function of frequency and canopy type at H-polarization. *IEEE Trans. Geosci. Remote Sens.* **42**, 786–794 (2004).
66. Konings, A. G., Rao, K. & Steele-Dunne, S. C. Macro to micro: microwave remote sensing of plant water content for physiology and ecology. *New Phytol.* <https://doi.org/10.1111/nph.15808> (2019).
67. Du, J. et al. A global satellite environmental data record derived from AMSR-E and AMSR2 microwave earth observations. *Earth Syst. Sci. Data Discuss.* <https://doi.org/10.5194/esd-2017-27> (2017).
68. Du, J., Kimball, J. S., Jones, L. A. & Member, S. Passive microwave remote sensing of soil moisture based on dynamic vegetation scattering properties for AMSR-E. *IEEE Trans. Geosci. Remote Sens.* **54**, 597–608 (2015).
69. Du, J. et al. A global satellite environmental data record derived from AMSR-E and AMSR2 microwave Earth observations. *Earth Syst. Sci. Data* **9**, 791–808 (2017).
70. Jones, L. A. et al. Satellite microwave remote sensing of daily land surface air temperature minima and maxima from AMSR-E. *IEEE J. Sel. Top. Appl. Earth Obs. Remote Sens.* **3**, 111–123 (2010).
71. Olson, D. M. et al. Terrestrial Ecoregions of the World: A New Map of Life on Earth: a new global map of terrestrial ecoregions provides an innovative tool for conserving biodiversity. *BioScience* **51**, 933–938 (2001).
72. Zar, J. H. in *Biostatistical Analysis* 1st edn, 185–205 (Prentice-Hall International, 1984).
73. Fox, J. et al. Package ‘car’ (R Foundation for Statistical Computing, 2012).
74. Fox, J., Friendly, M. & Weisberg, S. Hypothesis tests for multivariate linear models using the car package. *R J.* **5**, 39–52 (2013).
75. Dormann, C. F. et al. Methods to account for spatial autocorrelation in the analysis of species distributional data: a review. *Ecography* **30**, 609–628 (2007).
76. Pinheiro, J. et al. nlme: linear and nonlinear mixed effects models. R package v.3.1-117 (R Foundation for Statistical Computing, 2014).
77. R Core Team *R: A Language and Environment for Statistical Computing* (R Foundation for Statistical Computing, 2012).

Acknowledgements

All correspondence and requests for materials should be addressed to W. Anderegg. W.R.L.A. acknowledges funding from the David and Lucille Packard Foundation, NSF Grants 1714972 and 1802880, and the USDA National Institute of Food and Agriculture, Agricultural and Food Research Initiative Competitive Programme, Ecosystem Services and Agro-ecosystem Management, grant no. 2018-67019-27850. A.T.T. acknowledges funding from the USDA National Institute of Food and Agriculture, Agricultural and Food Research Initiative Competitive Programme grant no. 2018-67012-31496 and the University of California Laboratory Fees Research Program Award No. LFR-20-652467. A.G.K. acknowledges funding from the NASA Carbon Cycle Science Program, and through the New Investigator Program (award 80NSSC18K0715), and from NOAA grant NA17OAR4310127.

Author contributions

W.R.L.A., A.T.T. and G.B. designed the study. A.G.K. and J.S. provided key datasets. W.R.L.A. and A.T.T. analysed the data. W.R.L.A. wrote the first draft of the paper, and all authors contributed to writing and revising the manuscript.

Competing interests

The authors declare no competing interests.

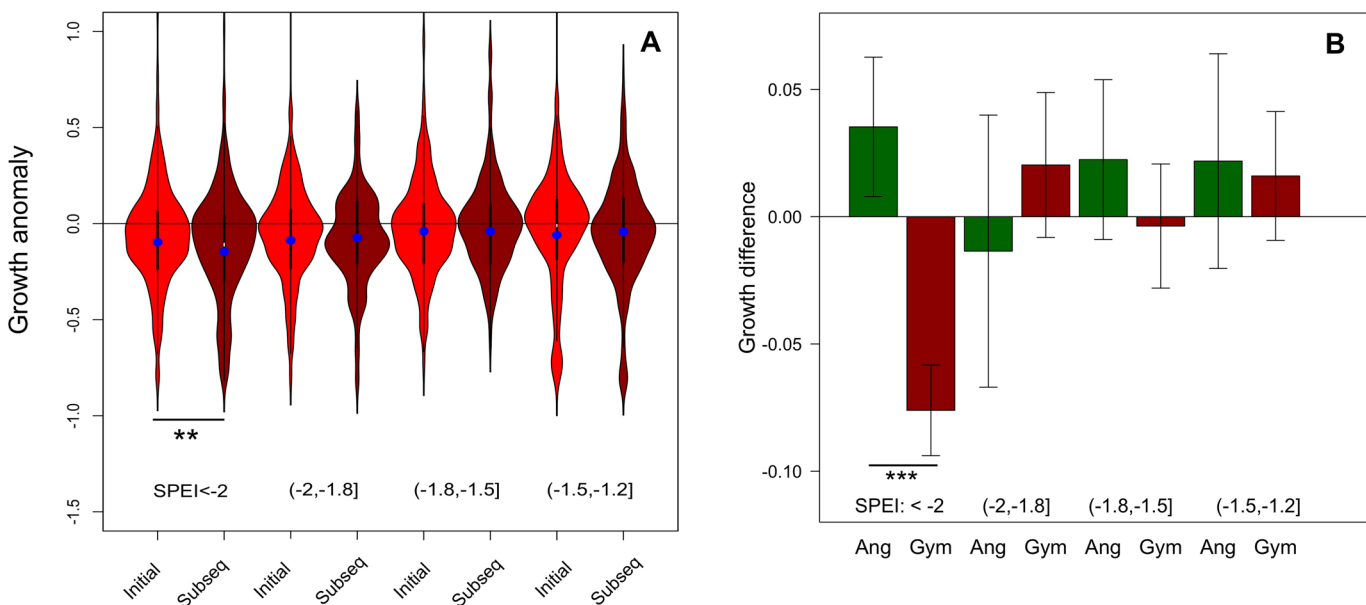
Additional information

Extended data is available for this paper at <https://doi.org/10.1038/s41558-020-00919-1>.

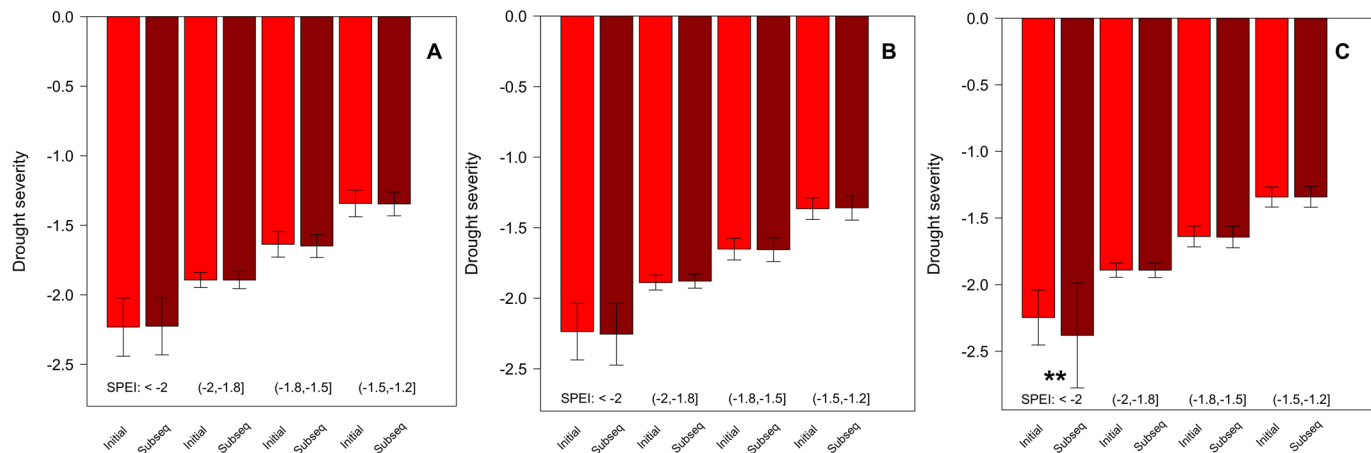
Correspondence and requests for materials should be addressed to W.R.L.A.

Peer review information *Nature Climate Change* thanks Adriaan J. Teuling, Alistair Jump and Tao Zhang for their contribution to the peer review of this work.

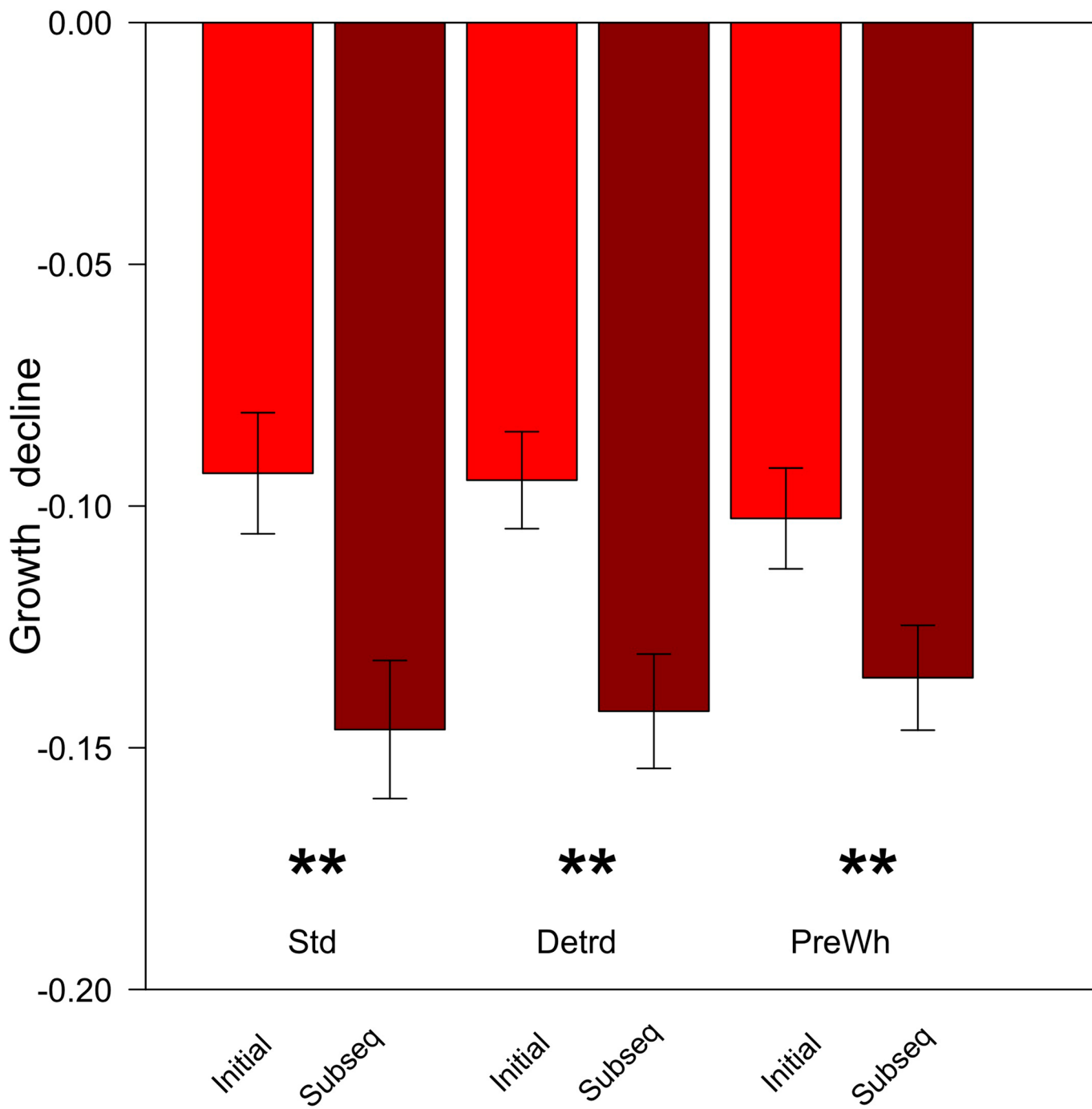
Reprints and permissions information is available at www.nature.com/reprints.



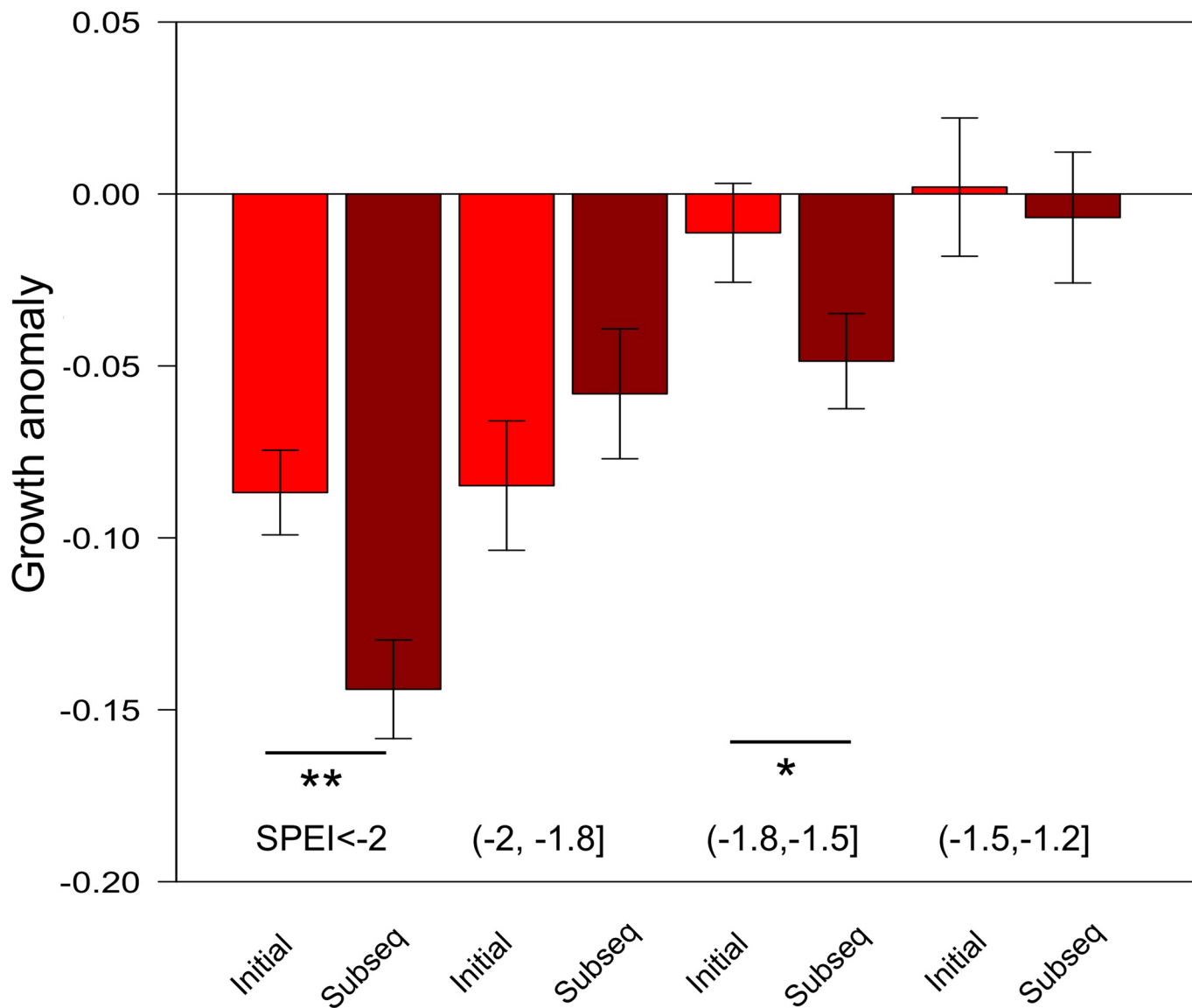
Extended Data Fig. 1 | Impacts of a subsequent drought are more deleterious than an initial drought for trees. Growth declines (Δ ring width index; **a**) from 1,208 sites in the International Tree-Ring Data Bank to an initial drought (Initial, light red) and subsequent drought (Subseq, dark red), categorized by drought severity of both droughts via the Standardized Precipitation Evapotranspiration Index (SPEI) thresholds. Identical data as Fig. 1a but shown as a violin plot. Blue dots are the mean. Numbers in italics are the number of chronologies in each bin. **b**, Growth declines differences from the International Tree-Ring Data Bank by clade where negative numbers indicate a more deleterious effect of the subsequent drought (left-to-right $N_{\text{chronologies}} = 106, 410, 40, 174, 56, 291, 34, 257$). Stars indicate statistically significant differences (* $p < 0.05$, ** $p < 0.01$, *** $p < 0.001$).



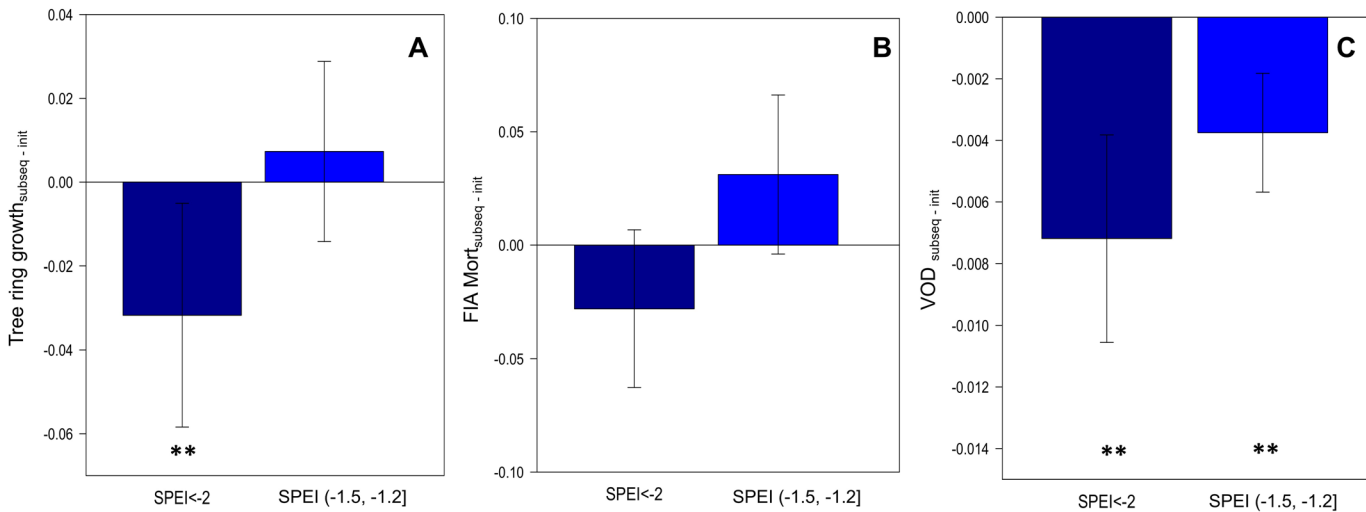
Extended Data Fig. 2 | Drought severity was typically similar between initial and subsequent droughts. Drought severity differences for tree-ring (a), forest inventory (b), and vegetation optical depth (c) data. Initial drought (ID, light red) and subsequent drought (SD, dark red) drought severity of both droughts via the Standardized Precipitation Evapotranspiration Index (SPEI) thresholds. For sample sizes, see Figs. 1a, b, 3a. Error bars indicate ± 1 S.D. Stars indicate statistically significant differences (* $p < 0.05$, ** $p < 0.01$).



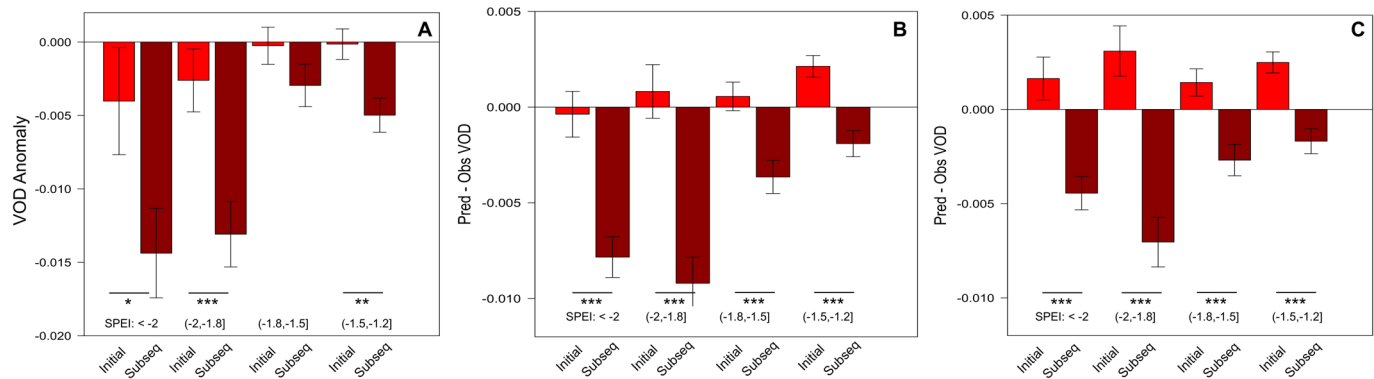
Extended Data Fig. 3 | Growth decline results were consistent across multiple tree-ring analysis methods. Ring width difference during drought compared to average growth for an initial drought (ID, light red) and subsequent drought (SD, dark red) at SPEI < -2 drought severity threshold for the standardized (that is standard detrended ".crn" file presented in ITRDB) tree-ring chronology ("Std"; as in Fig. 1), a consistent spline de-trending method applied to all chronologies ("Detrd"), and a detrended and "prewhitened" (that is autoregressive model removed) ("PreWh"). Error bars indicate ± 1 S.E.M. Stars indicate statistically significant differences (** $p < 0.01$).



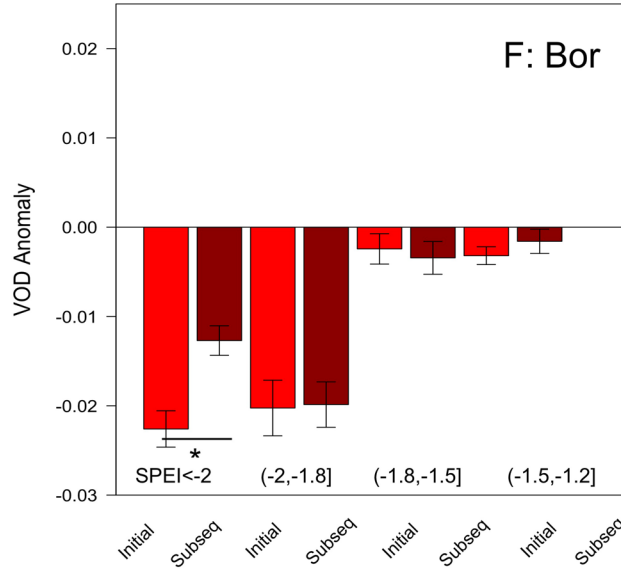
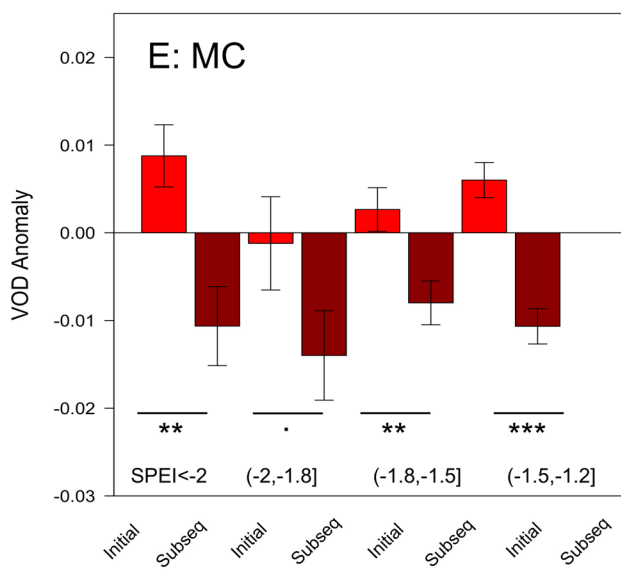
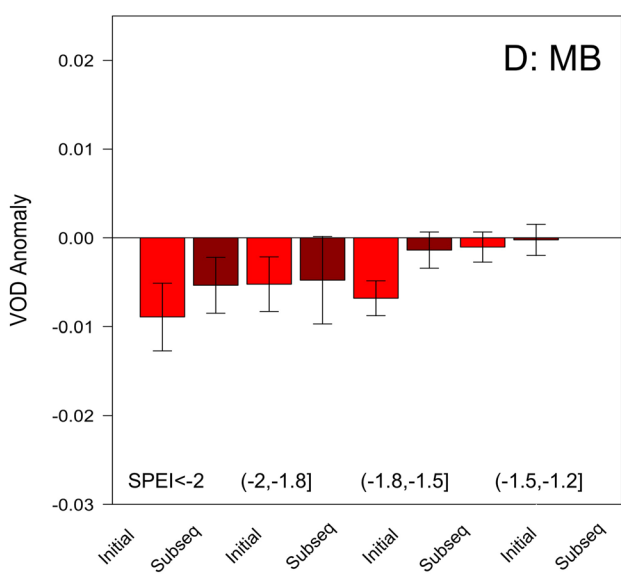
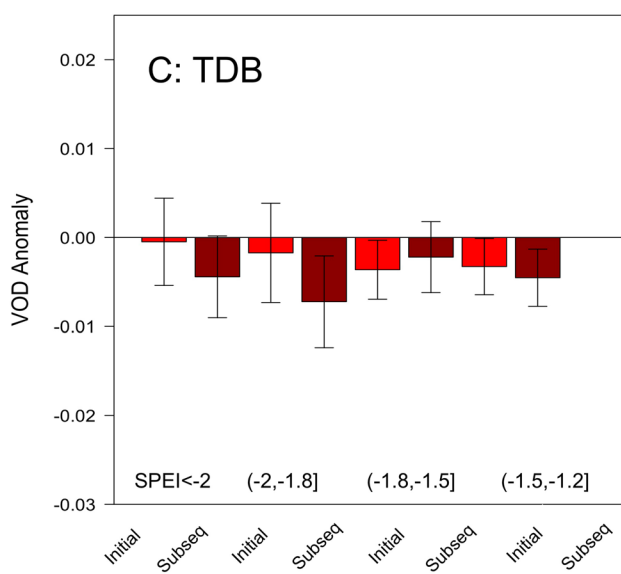
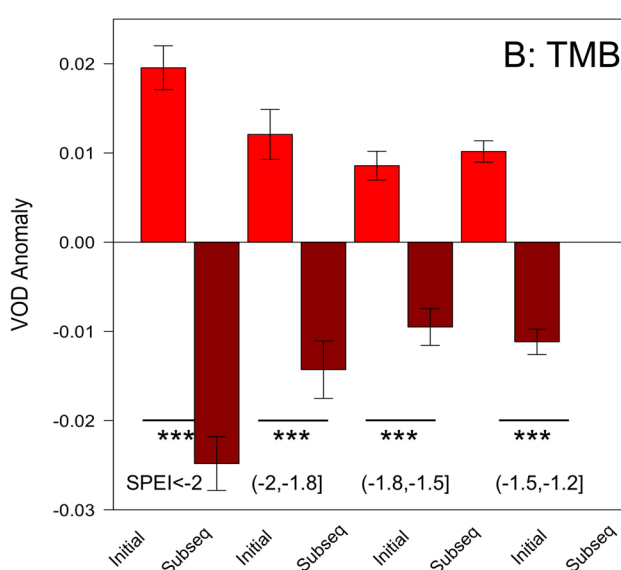
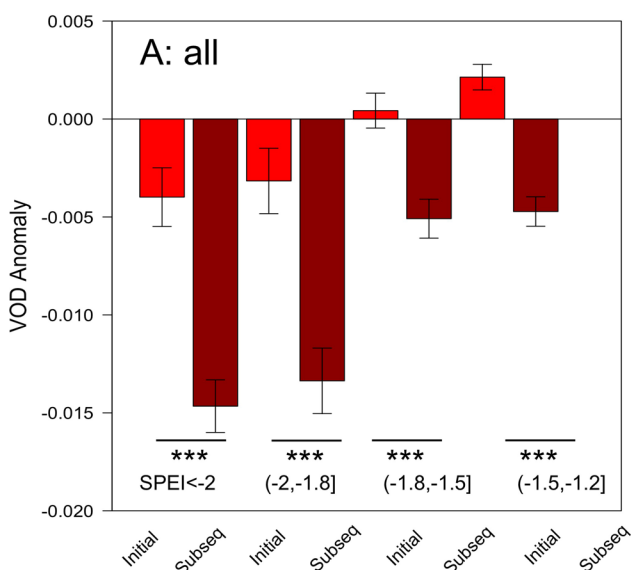
Extended Data Fig. 4 | Impacts of a subsequent drought are more deleterious than an initial drought for trees. Growth declines (Δ ring width index) from 1,208 sites in the International Tree-Ring Data Bank to an initial drought (Initial, light red) and subsequent drought (Subseq, dark red), categorized by drought severity of both droughts via the Standardized Precipitation Evapotranspiration Index (SPEI) thresholds. For multi-year droughts, the first year of the drought was analyzed. Error bars indicate ± 1 standard error. Stars indicate statistically significant differences (* $p < 0.05$, ** $p < 0.01$).



Extended Data Fig. 5 | All results are robust to accounting for spatial autocorrelation. **a**, Difference in tree ring width index between a subsequent drought (SD) and an initial drought (SD) at two drought severity thresholds, where negative numbers indicate a subsequent drought is more harmful. **b**, Difference in mortality in forest inventory plots between a subsequent drought (SD) and an initial drought (SD) at two drought severity thresholds, where positive numbers indicate a subsequent drought is more harmful. **c**, Difference in vegetation optical depth (VOD) anomaly between a subsequent drought (SD) and an initial drought (SD) at two drought severity thresholds, where negative numbers indicate a subsequent drought is more harmful. Error bars indicate $\pm 1\text{S.E.M}$. Stars indicate statistically significant differences from zero (* $p < 0.05$, ** $p < 0.01$).

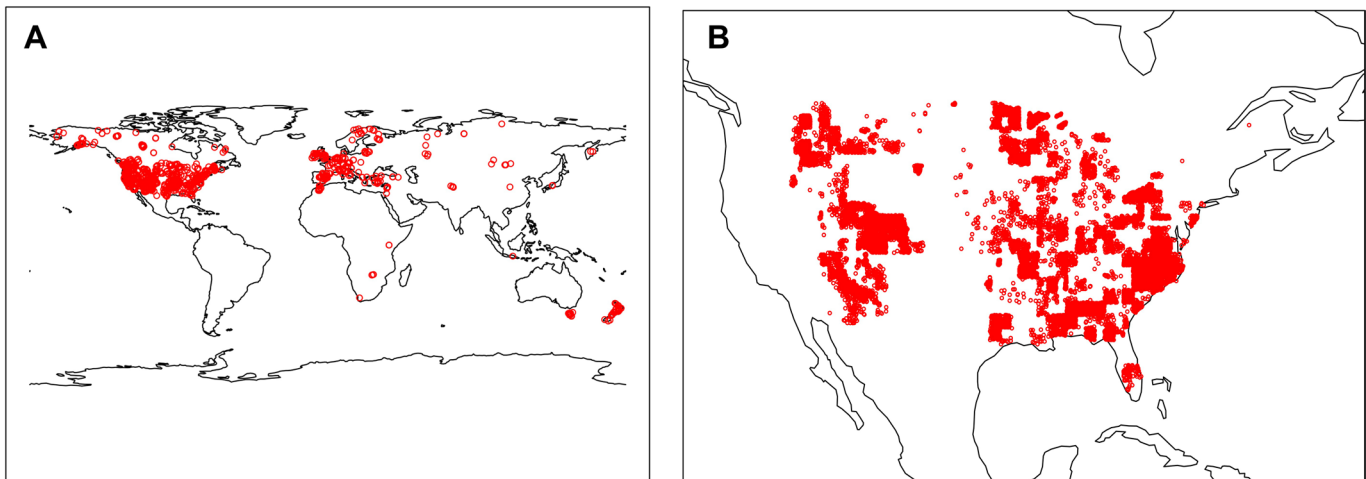


Extended Data Fig. 6 | Ecosystem impacts of multiple droughts are robust to accounting for drought severity differences. Vegetation optical depth (VOD) anomaly (**a**) in response to an initial drought (Initial, light red) and subsequent drought (Subseq, dark red), categorized by drought severity of both droughts via the Standardized Precipitation Evapotranspiration Index (SPEI) thresholds. Panels (**b**) and (**c**) show the predicted minus observed VOD anomalies after constraining a grid cell specific linear (**b**) and quadratic (**c**) regression between SPEI and VOD anomaly. Error bars indicate $\pm 1\text{S.E.M}$. Stars indicate statistically significant differences (** $p < 0.01$, *** $p < 0.001$).

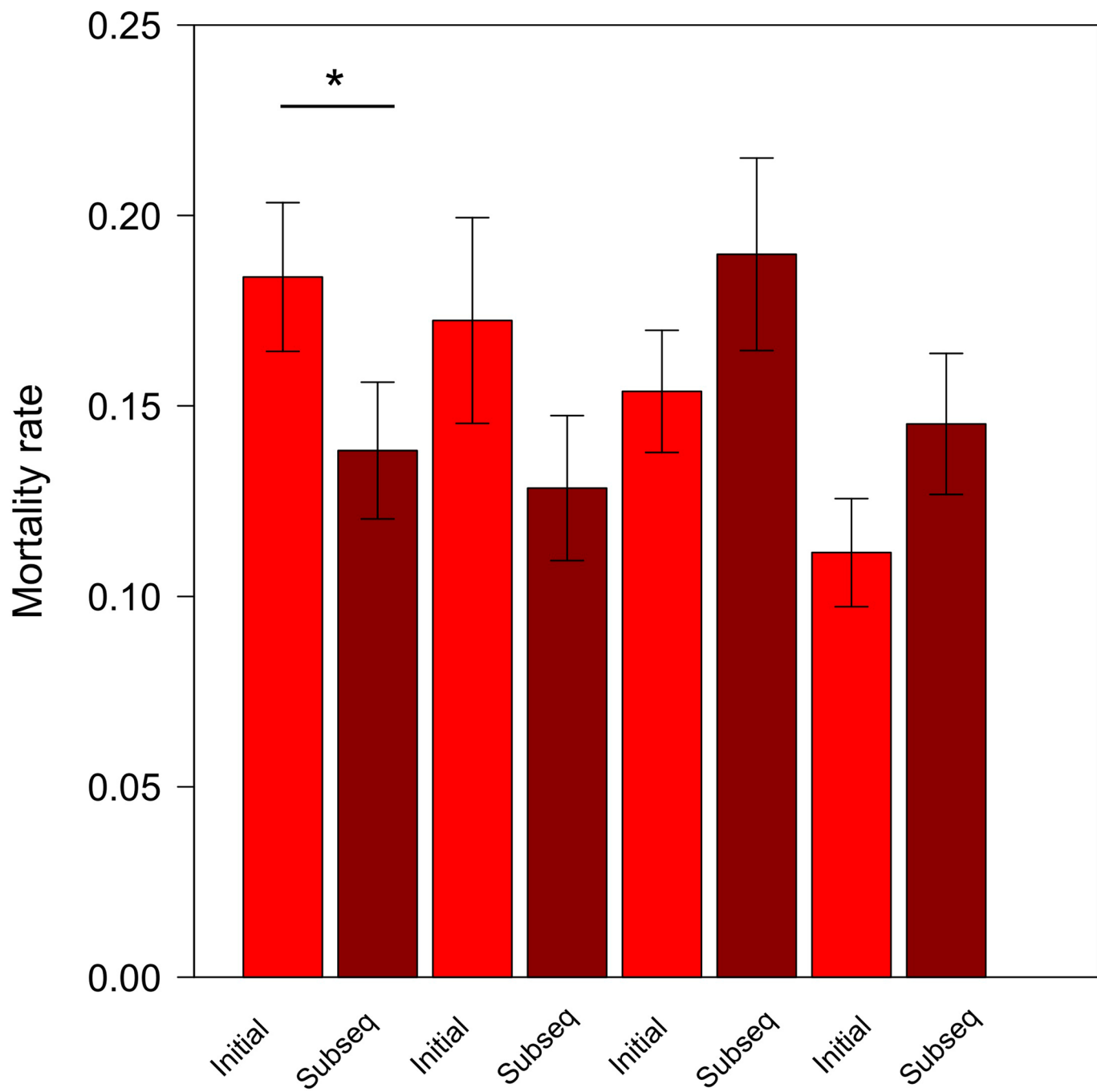


Extended Data Fig. 7 | See next page for caption.

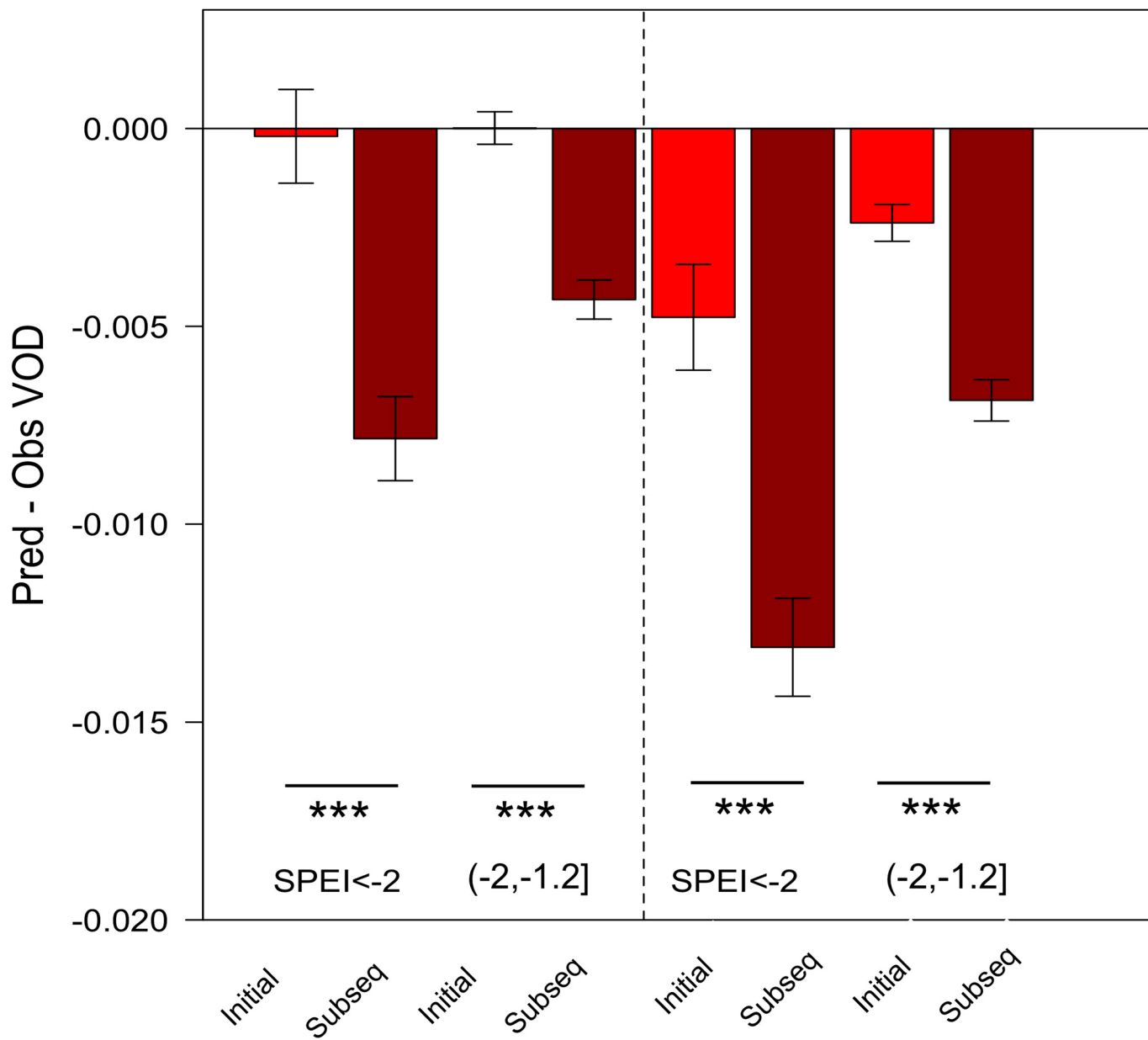
Extended Data Fig. 7 | Ecosystem impacts of a subsequent drought are more deleterious than an initial drought, accounting for potential drought legacy effects. Vegetation optical depth (VOD) anomaly in response to an initial drought (Initial, light red) and subsequent drought (Subseq, dark red), categorized by drought severity of both droughts via the Standardized Precipitation Evapotranspiration Index (SPEI) thresholds. All analyses used a 3+ year gap between initial and subsequent droughts. For biome definitions, see Fig. 3c. Error bars indicate $+/- 1$ standard error. Stars indicate statistically significant differences following other figures.



Extended Data Fig. 8 | Analysis included broad geographic coverage of tree growth and mortality. Geographical coverage of (a) the International Tree-Ring Data Bank (ITRDB) tree-ring chronologies, and (b) U.S. Forest Inventory and Analysis (FIA) long-term inventory plots included in this analysis.



Extended Data Fig. 9 | Similar qualitative mortality patterns are observed in terms of mortality differences between initial and subsequent droughts.
This figure presents these patterns when excluding FIA mortality data from Intermountain West states ($N_{\text{plots}}: 2848, 1270, 2559, 920$; $N_{\text{grid-cells}}: 99, 43, 93, 54$ left-to-right bar pairs). Figure legend otherwise the same as in Fig. 1b.



Extended Data Fig. 10 | The deleterious impacts of subsequent droughts are robust to accounting for temporal trends. Vegetation optical depth (VOD) responses to initial (Initial) and subsequent (Subseq) droughts are robust to accounting for potential trends in VOD. Left of the dashed line indicates the approach of selecting for grid cells without significant trends, while right of the dashed lines indicate detrending individual grid cells at the outset. Otherwise, legend is identical to Fig. 3a. Stars indicate statistically significant differences (**p < 0.001).